Heliyon

Structure and stability of hcp iron carbide precipitates: A first-principles study

C.M. Fang [a,b,*], M.A. van Huis [b]

[a] *Brunel Centre for Advanced Solidification Technology (BCAST), Brunel University London, Kingston Lane, Uxbridge, Middlesex, UB8 3PH, UK*

[b] *Soft Condensed Matter, Debye Institute for Nanomaterials Science, Utrecht University, Princetonplein 5, 3584CC Utrecht, The Netherlands*

* Corresponding author at:

E-mail address: Changming.Fang@brunel.ac.uk (C.M. Fang).

Abstract

Hexagonal close-packed (hcp) iron carbides play an important role in steel processing and in steel products. The recent discovery of novel ultrafine (2–5 nm) iron carbide (ε'-$Fe_{2+x}C$) precipitates in TRIP steel sheds a new light on the hcp family of carbides. Here we present a first-principles study on the relative stability, and the electronic, magnetic properties of the ε'-Fe_2C phases. Different stackings of Fe-sheets and orderings of C atoms were investigated and compared with experimental data and with Jack's model. We find very favorable formation enthalpies for these new members of the hcp family, and we present a first-principles-refined model for the crystal structure of the ultrafine Fe(C) precipitates. These findings are useful for the characterization of nano-sized iron carbide precipitates, for understanding their role in the microstructure of steels, and for the design of novel steels having even more desirable properties.

Keywords: Condensed matter physics, Engineering, Materials science

1. Introduction

The hexagonal-close-packed (hcp) ε-$Fe_{2+x}C$ phases have long been recognized to play an important role in various processes of steel manufacturing, and have a strong influence on the properties of the products [1, 2, 3, 4]. Therefore,

knowledge about these precipitates is useful for the development of steels having desirable properties [1, 2, 3, 4, 5, 6, 7, 8, 9, 10, 11, 12, 13, 14, 15, 16, 17, 18]. As early as in the 1950's, Hofer and Cohn studied the tempering processes of quenched martensite steels and identified the formation of the ε-$Fe_{2+x}C$ phase [8, 9, 10, 11, 12, 13, 14]. Jack proposed several structural models for the ε-$Fe_{2+x}C$ precipitates [11, 12, 13, 19, 20]. Recently, in the characterization of TRIP (Transformation induced plasticity) steels, Tirumalasetty et al. observed a new type of ultra-fine, disc-shaped Fe(C) precipitates with sizes of 2–5 nm [8]. These novel precipitates possess a hexagonal crystal structure with lattice parameters $a = 5.73$ Å, $c = 12.06$ Å. They are in a well-defined Pitsch-Schrader (P-S) orientation relationship with the basal plane of the precipitate parallel to the [110] habit plane of the surrounding ferritic (body centered cubic iron, bcc-Fe) matrix and are expected to contribute considerably to the strengthening of these steels [8]. Review of the literature shows that the crystal structure of these novel precipitates is different from existing models [5, 9, 10, 12, 13, 14, 15, 16, 17, 18, 19, 20, 21, 22]. We designate this new type of precipitates as ε'-$Fe_{2+x}C$ throughout this paper. Unfortunately, although the lattice parameters were determined, the TEM observations cannot provide decisive information on the chemical concentration, Fe stacking and C ordering, partially due to the nano-sizes of the precipitates (with thicknesses of 2–5 nm) and the fact that they are embedded in another material. Therefore theoretical methods, especially parameter-free first-principles methods, can be very helpful for elucidating the crystal structure. Structural relaxation and total energy calculations provide accurate information about the crystal structures, chemical bonding, and relative stability of crystals at the ground state, and have been successfully applied to many iron carbides [12, 13, 14, 15, 16, 17, 18, 19, 20, 21].

Here we summarized the literature on the hexagonal iron carbides in Table 1 from first-principles calculations for hcp Fe_2C and related phases [19, 20, 21, 22]. All the hcp Fe_2C structural models are variations on the simple structure proposed by Jack in the early 1950s, which is hexagonal with $a_0 \sim 2.8$ Å, $c_0 \sim 4.2$ Å. This cell (Jack-1) contains two Fe atoms at (0,0,0) and (1/3,2/3,1/2) and one C at (2/3, 1/3, 1/4) or (2/3, 1/3, 3/4), as shown in Fig. 1a and Table 1 [19, 20, 21, 22, 23]. The widely used conventional ε-$Fe_{2+x}C$ cell was built with $a_1 = a_0 \sqrt{3} \sim 4.8$ Å and $c_1 = c_0 \sim 4.2$ Å. It contains 6 Fe atoms and 3C atoms (Fig. 1). This structural model was named Jack-2 [21, 22]. This ε-Fe_2C lattice can be easily transferred into the orthorhombic η-Fe_2C phase [13, 21, 22]. Experimentalists also observed extra diffraction lines for the hcp iron carbide precipitates (ε-$Fe_{2+x}C$) [9, 10, 12, 13, 14, 15, 16, 17, 18, 19, 20]. A larger hexagonal super-cell with $a' = 2\sqrt{3}\, a_0 \sim 9.6$ Å, $c' = c_0$ was used to solve the crystal structure of different carbon concentrations, e.g. $x \sim 2.4$ [9, 10, 13, 19, 20, 21, 22]. This structural model was named Jack-3 [21, 22]. Based on the recent TEM observations [8] here we

Table 1. Calculated results for the new ε'-Fe_2C phase and related phases (see text). The results for cementite θ-Fe_3C are included for the sake of comparison. The relationships between the different structural models are indicated. All the lattice parameters of the ε-Fe_2C phases are converted to the primitive cell (isostructural to the Jack-1 model) [19, 20, 21, 22]. Also the calculated lattice parameters and formation enthalpies of several frequently observed iron carbides are included. *With the experimental lattice parameter [8].

Model	Phase/symmetry	Lattice relations	Lattice par. (Å)	ΔE_f (meV/atom)	References
ε-Fe_2C	Jack-1	$a_1 = a_o$ $c_1 = c_o$	$a_o = 2.834$ $c_o = 4.1673$	+120.4	[21, 22]
	Jack-2	$a_2 = \sqrt{3}a_o$ $c_2 = c_o$	$a_o = 2.773$ $c_o = 4.295$	+35.3	[21, 22]
	Jack-3	$a_3 = 2\sqrt{3}\,a_o$ $c_3 = c_o$	$a_o = 2.771$ $c_o = 4.291$	+27.9	[21, 22]
ε'-Fe_2C	hcp	$a' = 2\,a_o$ $c' = c_o$	$a_o = 2.744$ $c_o = 4.267$	+26.7	present work
η-Fe_2C	Orth.		$a_\eta = 4.707$ $b_\eta = 4.280$ $c_\eta = 2.824$	+17.3	[21, 41]
θ-Fe_3C	Orth.		$a_\theta = 5.037$ $b_\theta = 6.720$ $c_\theta = 4.482$	+20.6	[21, 41]
ε-Fe	Hcp		$a_0 = 2.523$ $c_0 = 4.375$	+194.7	present work
Fe ordering					
ε'-Fe_2C (hcp)	Fe series: ABABAB	$a' = 2\,a_o$ $c' = c_o$	$a_o = 2.865$ * $c_o = 4.020$	+52.4	Present work
h-Fe_2C	Fe series: ABCBAB	$a' = 2\,a_o$ $c' = c_o$	$a_0 = 2.704$ $c_0 = 4.342$	+62.5	Present work
h-Fe_2C	Fe series: ABCBAC	$a' = 2\,a_o$ $c' = c_o$	$a_0 = 2.660$ $c_0 = 4.377$	+162.0	Present work

build a new structure for the ε'-$Fe_{2+x}C$ precipitates with lattice parameters $a' = 2a_0$, and $c' = c_0$ (Table 2). In the present paper we present our first-principles modeling for the novel ε'-$Fe_{2+x}C$ precipitates based on the experiments [8]. Various possibilities for stacking of Fe-sheets were taken into consideration. We also considered the lattice as confined by the surrounding ferrite matrix. The possible formation and transformation of this ε'-$Fe_{2+x}C$ precipitate is discussed, followed by a summary of the results.

2. Calculation

From the literature, it is well-established that all the Fe-rich iron carbides are metastable relative to the elemental solids (ferrite and graphite) [11, 12, 13, 21, 22, 23, 24, 25, 26, 27, 28]. To have a measure of the relative stability of iron carbides
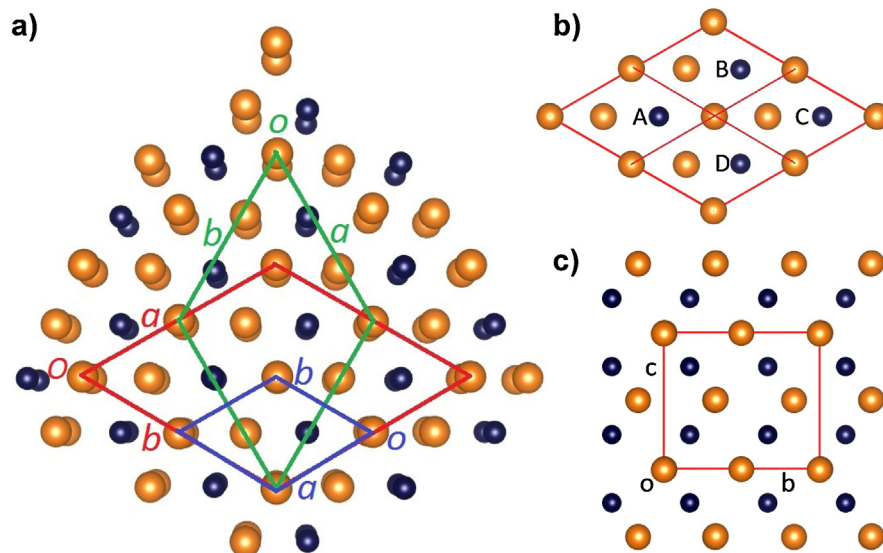
Fig. 1. (a) The schematic $a_0 \times b_0$ in-plane structure for model Jack-1 (primitive cell, blue lines), its relationship with the conventional model Jack-2 (dark green lines), and with the new model for ε'-Fe$_2$C cell (red lines) (1a). Schematic structure for the ε'-Fe$_2$C phase with the possible C sites along the (001) orientation (b) and along the (100) orientation (c). The large filled golden spheres represent Fe atoms, and the small black spheres possible C sites. In subfigure (b), there are two layers of C atoms in between the Fe layers. The labels A, B, C, D represent C sites in one layer (z ~ 1/4) and A', B', C', and D' for possible C sites in another layer (z ~ 3/4), as shown in 1c.

Table 2. Calculated electronic and magnetic configurations (EC and MC respectively) for ε'-Fe$_2$C from the DFT lattice parameters in comparison with related phases.

Phase	Chemical bonding	EC (electrons), MC and M (μ_B/atom)
hcp-Fe	Fe-Fe 2.52 (×6) 2.63 (×6)	EC: $4s^{0.05}\,4p^{0.55}\,3d^{6.33}$ MC: $4s^{-0.01}\,4p^{-0.04}\,3d^{2.58}$ Moment: 2.58/Fe,
ε'-Fe$_2$C	Fe-C: 1.92 (×2), 1.94 -Fe: 2.52, 2.62, 2.72 (×4) 2.74 (×4)	EC: $4s^{0.49}\,4p^{0.74}\,3d^{6.58}$ MC: $4s^{-0.01}\,4p^{-0.02}\,3d^{1.68}$ M: 1.66/Fe, −0.13/C
η-Fe$_2$C	Fe-C: 1.92 (×2), 1.94 -Fe: 2.59 (×2), 2.71 (×4) 2.74 (×4)	EC: $4s^{0.48}\,4p^{0.74}\,3d^{6.58}$ MC: $4s^{0.00}\,4p^{-0.02}\,3d^{1.69}$ M: 1.68/Fe, −0.13/C

with respect to the elemental solids, the formation energy (ΔE_f) per atom of iron carbide (Fe$_m$C$_n$) is employed, and is defined as [21, 22, 26, 27, 28]:

$$\Delta E_f = [E(\text{Fe}_m\text{C}_n) - (m\,E(\text{Fe}) + n\,E(\text{C}))]/(n + m), \tag{1}$$

At temperature $T = 0$ K and pressure $p = 0$ Pa, the enthalpy difference is equal to the energy difference, or $\Delta H(Fe_mC_n) = \Delta E(Fe_mC_n)$, when the zero-point vibration contribution is ignored.

We employ the first-principles' Vienna *Ab initio* Simulation Package (VASP) [29, 30, 31] for all the calculations. This code employs Density-Functional Theory (DFT) within the projector-augmented wave (PAW) method [32, 33]. The generalized gradient approximation (GGA) formulated by Perdew, Burke and Ernzerhof (PBE) [34] was employed for the exchange and correlation energy terms because the spin-polarized GGA approximation describes spin-polarized 3d metals such as Fe and related compounds better than the local (spin-polarized) density approximation (LDA) [35, 36]. Former systematic studies also showed that the DFT-GGA approximation describes the iron and iron carbides well [36]. The cut-off energy of the wave functions was set at 500 eV and the cut-off energy of the augmentation functions was set at 650 eV. The electronic wave functions were sampled on a $10 \times 10 \times 12$ grid with 98–337 k-points, or on a $10 \times 10 \times 4$ grid with 70–204 k-points, in the irreducible Brillouin zone (BZ) of $\varepsilon\text{-}Fe_{2+x}C$ structure with a short c-axis ($c = c_0$) or supercell ($c = 3c_0$) depending on the symmetry, using the Monkhorst–Pack method [37]. The k-mesh has a $24 \times 24 \times 24$ grid with 364 points in the irreducible BZ for α-Fe and the diamond phase of carbon. Structural optimizations were performed for both lattice parameters and coordinates of atoms. For the calculations of local electronic configurations and partial density of states of the atoms, Wigner–Seitz radii of 1.4 Å for Fe and 1.0 Å for C were used in the present calculations, respectively. Note that Fe 3d electrons exhibit an itinerant character, and in principle belong to the whole crystal. However, we can decompose the plane waves in the sphere and obtain Fe 3d components in the spheres for both the spin-up (or majority) and spin-down (minority) directions. In this way a local magnetic moment is obtained which is the difference of the number of spin-up electrons and spin-down electrons in the sphere. Different k-meshes and cut-off energies were used for the waves and augmentation waves, respectively. Tests showed a good convergence (<1 meV per atom).

3. Results and discussion

The calculations for the elemental solids provide the same results as our former work [21, 22]. We performed calculations for the diamond phase of carbon since the present DFT-GGA approximation can't describe the van der Waals interaction between the graphene sheets in the ground state graphite. Then an energy correction was made to get the correct total valence electron energy of graphite as one reference, as described in references [21, 22].

Fig. 1 shows the schematic structures of the new ε'-$Fe_{2+x}C$ phase which has a hexagonal lattice cell with parameters $a' = 2a_0$, $c' = c_0$. The eight Fe atoms form two layers of hexagonal sheets at fractional coordinates $z = 0$ and $z = 0.5$. There are eight possible octahedral sites for C atoms, which are labeled with A, B, C, D for C atoms at $z \sim 0.25$, and correspondingly A', B', C', D' for $z \sim 0.75$ (Fig. 1b and c). Fig. 2 shows the calculated formation energies according to Eq. (1). Different possible configurations were taken into consideration. Table 1 includes the lattice parameters, and the formation energy of ε'-Fe_2C, as well as a comparison with other phases of the same chemical composition, or having similar composition.

First we discuss the structure and electronic (magnetic) properties of the ε-Fe phase. ε-Fe exhibits a complicated (spiral) magnetic structure [38, 39, 40]. Cohen and Mukherjee studied the non-collinear magnetism in ε-Fe and found energetically small non-collinear effects [38]. In order to be consistent with other calculations, we performed calculations for ε-Fe as a ferro-magnet. The calculated results are shown in Tables 1 and 2, and in Figs. 2 and 3.

We now discuss the general trend of the formation energy for ε'-$Fe_{2+x}C$, starting from the high value of ferromagnetic ε-Fe (Table 1). As shown in Fig. 2, with increasing C concentration, the formation energy decreases strongly till reaching composition ε'-Fe_2C which has a formation energy as low as 26.7 meV/atom, close to that of model Jack-2 for ε-Fe_2C (27.9 meV/atom) calculated using the same method and settings [21, 22]. However, it is still higher than that of the orthorhombic phase η-Fe_2C. Further addition of C into the structure of ε'-Fe_2C leads to a strong increase of the formation energy (Fig. 2). This indicates that the upper limit of the C concentration is $x_C = 1/3$ (0.3333) according to Eq. (1) with formula ε'-Fe_2C.

As shown in Fig. 2, the ordering of C atoms has a strong impact on the formation energies of the ε'-$Fe_{2+x}C$ phases. In the case of ε'-Fe_4C which contains two C atoms in the cell, there are five independent (AA', AB, AB', AC, AC') arrangements (Fig. 1). Translation symmetry operation further reduces the number of independent arrangements (AB = AC and AB' = AC'). The calculations showed that the AA' configuration is very instable (about 2 eV/cell higher than the others). The configuration AB' or AC' with C atoms in different layers is the most stable, while the AB/AC configuration, having the C atoms in one layer, has an intermediate stability (Fig. 2a). The rule that C atoms are preferably distributed in different layers and not on top of each other, applies to the other chemical compositions of ε'-$Fe_{2+x}C$ as shown in Fig. 2a. For ε'-Fe_2C, the upper limit of C concentration, the four C atoms are distributed evenly in the two interstitial layers, as clearly shown in Fig. 2a. With increasing C concentration, the length of the *a*-axis increases, whereas the length of the *c*-axis deceases somewhat up to ε'-Fe_2C.
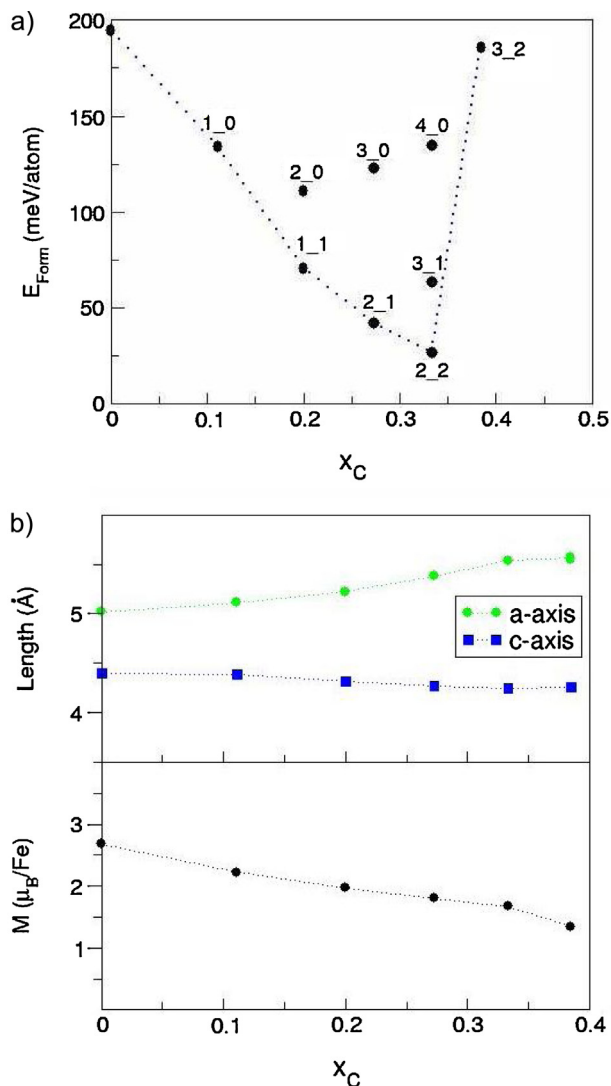
Fig. 2. The calculated formation energies (a) for the ε'-$Fe_{2+x}C$ phases and the size of the a- and c lattice parameters, as well the magnetic moments (b). The dotted line connecting the lowest energies is drawn to guide the eye. The labels n_m in Fig. 2a represent the number of C atoms in the first_second layer. The horizontal axis is the C concentration, $x_C = n/(m + n)$ in the formula Fe_mC_n.

For ε'-Fe_2C_{1+y}, the length of the c-axis increases again probably due to the fact that the additional C atoms are situated on top of the other two C atoms in other layers.

We make the following remarks on the symmetry of ε'-Fe_2C. The above calculations showed that for the most stable configurations, the 4 C atoms will be evenly distributed over the two interstitial octahedral sites. The lattice parameters are still hexagonal with the point group being D_{2h}. Structural relaxation showed that the C atoms still prefer the original sites, but that this is accompanied by a distortion of the Fe sheets. For the configuration with homogenous distribution (ordering 2_2 in Fig. 2), the Fe sublattice shows distortion along $(x, -x, z)$ (with x
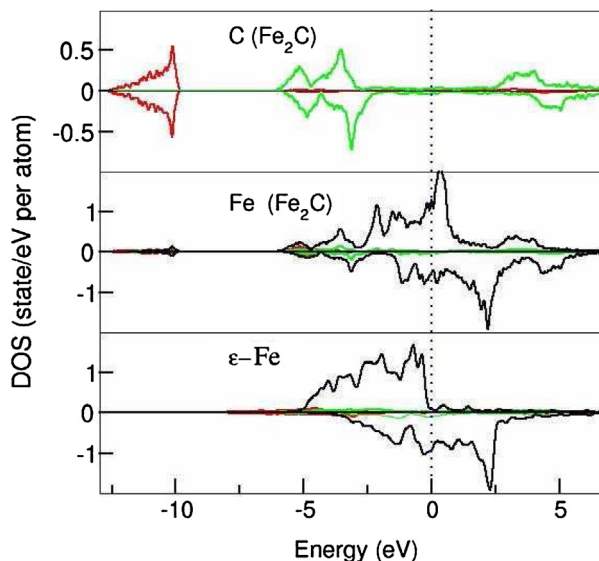
Fig. 3. Calculated partial density of states (pDOS) for Fe and C atoms/ions in ε'-Fe$_2$C and ε-Fe. The red lines represent s states, green p states, and black d states. The positive values are for spin-up (majority) electrons and minus for spin-down (minority) electrons.

~ 0.04 Å, $z \sim 0.03$ Å). As a result each C is coordinated by 6 Fe atoms with Fe-C interatomic distances of 1.92($\times 4$) Å and 1.94($\times 2$) Å. Each Fe atom is coordinated by 3 C and 9 Fe atoms (Table 2). The coordination in ε'-Fe$_2$C is very similar to those in η-Fe$_2$C as shown in Table 2. Therefore, it is expected that these two phases of iron carbide have a very similar bonding [40, 41].

The TEM observations [8] showed that the novel FeC precipitates a hexagonal super-cell with $a' = 5.73$ Å ($=2 a_0$) and $c' = 12.06$ Å ($\sim 3 c_0$) (here a_0 and c_0 are the lattice parameters of a primitive Fe$_2$C Jack-1 model, Fig. 1a). In this cell there are six layers of hexagonal Fe sheets. We remark that the length of c-axis should be 12.16 Å ($c' = 3\sqrt{2}\, a'$ according to the orientation relationship between the precipitates and its matrix, ferrite with axis length a') = 2.865 Å), instead of 12.06 Å from the TEM observations. The small difference is within the error of the method [8]. Our calculations also showed that such a small change has only a marginal impact on the formation energies (~ 2 meV/atom).

First we consider the stacking sequences for the Fe sheets. In the primitive hexagonal lattice, there are three Wyckoff positions each layer for the Fe, that is, A (0,0,z), B(2/3,1/3,z) and C (1/3,2/3,z). For the observed supercell, there are also three possible stacking possibilities for the six Fe sheets. That is, model (a) with Fe sheets in ABCABC order, based on the FCC structure, model (b) with an ABABAB sequence based on the hexagonal-close-packed (hcp) structure, and model (c) having an ABCBAB sequence, a mixture of fcc-based (a) and hcp-based (b).

We start with a configuration with half occupation corresponding to chemical composition Fe_4C, with one C in each layer, and end with full occupation at the structure of Fe_2C (Table 3). The calculations show that for the fcc-Fe based model (a), the formation energies are very high (above 100 meV/atom) for all C concentrations. For example, for Fe_4C the calculated formation energy is about 116 meV/atom, which is higher than that of γ'- Fe_4C (about 94 meV/atom) using the same method [41]. Fig. 4 shows the calculated formation energies for model (b) and model (c). The formation energies of both model (b) and model (c) decrease with increasing carbon concentration. The total energy calculations also showed that the formation energy of model (c) (mixture of fcc and hcp stacking) is about 30 meV/atom higher than that of model (b) in the chemical composition range that we are interested in. Therefore, we limit our discussion to model (b).

As shown in Figs. 2 and 4, the formation energy for ε'-phase decreases almost linearly with increases C concentration until $x_C = 1/3$, both for the small cell and for the supercells. Again ε'-Fe_2C has the highest stability. Addition of C into ε'-Fe_2C leads to an increase of the formation energy. Fig. 4 also includes the calculated formation energy of the ε'- phase with the lattice parameters fixed to those from the TEM observations. This represents the constraint effect of the matrix (ferrite) on the ε'-Fe_2C precipitates in the steel. The impact of lattice constraint on the formation energies is strong. As a whole, the lattice constraint leads to higher formation energy.

As shown in Fig. 3, the Fe atoms in ε-Fe are fully spin-polarized: for the spin-up electrons the Fe 3d states are almost fully occupied, while they are partially occupied for the spin-down electrons. This results in a large magnetic moment

Table 3. Optimal crystal structure model for the Fe(C) precipitate as predicted by the DFT calculations using the experimental lattice parameters [8].

Lattice parameter (Å) [8]	$a = 5.73$	$\alpha = 90°$				
	$b = 5.73$	$\beta = 90°$				
	$c = 12.06$	$\gamma = 120°$				
Space group	$P6_122$ (nr. 178)					

Atomic Coordinates

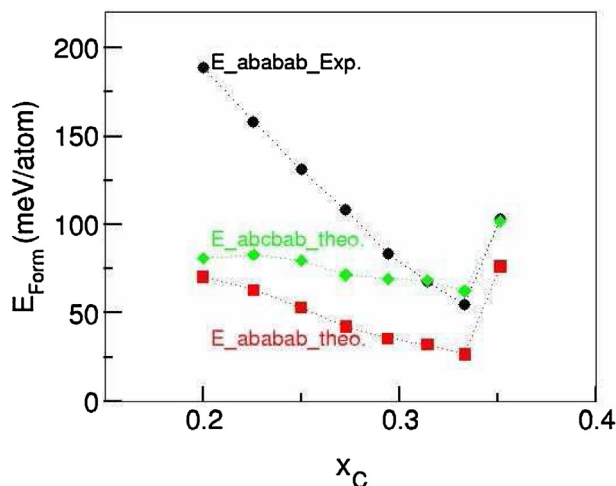| Atom	Wyckoff site	x	y	z	Overall B	Occupation
Fe1	12c	1/6	1/3	1/12	0	1.0
Fe2	6b	4/6	1/3	1/12		1.0
Fe3	6b	4/6	5/6	1/12		1.0
C1	12c	1/2	1/2	0		0.5
C1	6a	1/2	0	0		0.5
C1	6a	0	0	0		0.5

Fig. 4. Formation energies for 'model (b)' FeC_x with ABABAB stacking with relaxed lattice parameters (filled red spheres), and 'model (b)-exp' with lattice parameters fixed to the experimental values (black filled spheres). The calculated results for model (c) with ABCBAB stacking and with relaxed lattice parameters (filled green spheres), are included for comparison. The dotted lines are drawn to guide the eyes. The horizontal axis is the same as Fig. 2.

(about 2.6 μ_B/Fe). This solution of hcp_Fe provides a spin-polarization picture similar to that of α-Fe which has a magnetic moment of about 2.2 μ_B/Fe [42, 43, 44]. Addition of C atoms into ε-Fe causes admixture between Fe 4s, 4p, 3d and C 2p states as clearly shown in [40]. It is then expected that magnetic moment of the iron carbide will decrease with increasing C concentration. This picture can be easily seen from Table 2 and Fig. 3 from the comparison between ε-Fe$_\backslash$ and ε-Fe$_2$C. This trend is confirmed by our calculations for ε-Fe$_{24}$C$_n$: the magnetic moment decreases from 1.9 μ_B/Fe for n = 6 (x_C = 0.20) to about 1.6 μ_B/Fe for n = 12 (x_C = 0.3333) and for ε-Fe$_8$C$_n$ in Fig. 2b.

Our calculations are valid for the ground state of the phases. However the formation of the iron carbide precipitates takes place at high temperatures, for example at 1400 K, at which iron carbides form. In that case, thermal contributions such as configurational entropy may play a role. For example, if we consider that the configurational entropy for Fe$_{24}$C$_{12}$ is zero, then the independent configuration number Z is 6 for Fe$_{24}$C$_{11}$, is 6*5/2 = 18 for Fe$_{24}$C$_{10}$, and is 6*5*4/(2*3) = 20 for Fe$_{24}$C$_9$, if we ignore the energy differences due to the C2 ordering. Correspondingly, the entropy contribution at 1200 K is 0 eV/cell (or 0 meV/atom) for Fe$_{24}$C$_{12}$, 0.217 eV/cell (6.2 meV/atom) for Fe$_{24}$C$_{11}$, 0.327 eV/cell (or 9.89 meV/atom) for Fe$_{24}$C$_{10}$, and 0.362 eV/cell (or 11.0 meV/atom) for Fe$_{24}$C$_9$. Another conclusion is that the stability of the phase depends on the lattice dimensions: the calculated formation energy difference between Fe$_{24}$C$_{12}$ and Fe$_{24}$C$_{11}$ is 6.3 meV/atom for the computed fully relaxed lattices, 6.0 meV/atom

when they are confined to the computed lattice dimensions of ferrite, and 13.4 meV/atom when they are confined to the lattice dimensions obtained from the TEM observations. From Table 2, we expect that the chemical composition of the $Fe_{2+x}C$ precipitates is approximately centered at x = 0.05, yielding a composition of $Fe_{24}C_{11}$, being dependent on the local C concentration and the formation temperature.

4. Conclusions

From a careful consideration of available experimental data, diverse structural models were designed for the novel nano-sized hcp iron carbide (ε'-$Fe_{2+x}C$) precipitates in the TRIP steels, and simulated by first-principles DFT-GGA calculations. This results in a new structure for ε-Fe_2C. Furthermore, the total energy calculations predicted carbon deficiency in the precipitates that are formed at high temperature (Table 3). The present results make the already rich family of hcp FeC phases more complete, and also indicates the importance of, and the energy associated with the embedding of these ultrafine precipitates in the ferrite matrix.

Declarations

Author contribution statement

C.M. Fang: Conceived and designed the experiments; Performed the experiments; Analyzed and interpreted the data; Contributed reagents, materials, analysis tools or data; Wrote the paper.

M.A. van Huis: Conceived and designed the experiments; Analyzed and interpreted the data; Contributed reagents, materials, analysis tools or data; Wrote the paper.

Competing interest statement

The authors declare no conflict of interest.

Funding statement

Additional information

No additional information is available for this paper.

Acknowledgements

References

[1] M. Militzer, A synchrotron look at steel, Science 298 (2002) 975.

[2] H.K.D.H. Bhadeshia, TRIP-assisted steels? ISIJ Int. 42 (2002) 1059.

[3] G.K. Tirumalasetty, M.A. van Huis, C. Kwakernaak, J. Sietsma, W.G. Sloof, H.W. Zandbergen, Deformation-induced austenite grain rotation and transformation in TRIP-assisted steel, Acta Mater. 60 (2012) 1311.

[4] G.K. Tirumalasetty, M.A. van Huis, C. Kwakernaak, J. Sietsma, W.G. Sloof, H.W. Zandbergen, Unravelling the structural and chemical features influencing deformation-induced martensitic transformations in steels, Scr. Mater. 71 (2014) 29.

[5] E.V. Pereloma, I.B. Timokhina, K.F. Russell, M.K. Miller, Characterization of clusters and ultrafine precipitates in Nb-containing C–Mn–Si steels, Scr. Mater. 54 (2006) 471.

[6] E.V. Pereloma, K.F. Russell, M.K. Miller, I.B. Timokhin, Effect of pre-straining and bake hardening on the microstructure of thermomechanically processed CMnSi TRIP steels with and without Nb and Mo additions, Scr. Mater. 58 (2008) 1078.

[7] G.K. Tirumalasetty, M.A. van Huis, C.M. Fang, Q. Xu, F.D. Tichelaar, D.N. Hanlon, J. Sietsma, H.W. Zandbergen, Characterization of NbC and (Nb, Ti) N nanoprecipitates in TRIP assisted multiphase steels, Acta Mater. 59 (2011) 7406.

[8] G.K. Tirumalasetty, C.M. Fang, Q. Xu, J. Jansen, J. Sietsma, M.A. Van Huis, H.W. Zandbergen, Novel ultrafine Fe(C) precipitates strengthen transformation-induced-plasticity steel, Acta Mater. 60 (2012) 7160–7168.

[9] L.J.E. Hofer, E.M. Cohn, W.C. Peebles, The Modifications of the Carbide, Fe_2C; Their Properties and Identification, J. Am. Chem. Soc. 71 (1949) 189.

[10] L.J.E. Hofer, E.M. Cohn, Some reactions in the iron–carbon system: application to the tempering of martensite, Nature 167 (1951) 977.

[11] J.W. Christian V, The Theory of Transformation in Metals and Alloys, Pergamon Press, Oxford, 2002.

[12] H.J. Goldschmidt, A new iron boro-carbide, J. Iron Steel Inst. 160 (1948) 345.

[13] S. Nagakura, S. Oketani, Structure of transition metal carbides, Trans. Iron Steel Inst. Jpn. 8 (1968) 265.

[14] M. Ron, H. Shechter, S. Niedzwiedz, An introduction to mössbauer spectroscopy, J. Appl. Phys. 39 (1968) 265.

[15] R.H. Doremus, E.F. Koch, The precipitation of carbon from alpha-iron. 1. Electron microscopic study, Trans. Met. Soc. AIME 218 (1960) 591.

[16] M. Manes, A.D. Damick, E.M. Mentser, M. Cohn, J.L.E. Hofer, Hexagonal Iron Carbide as an Intermediate in the Carbiding of Iron Fischer—Tropsch Catalysts[1,2], J. Am. Chem. Soc. 74 (1952) 6207.

[17] B.G. Hyde, S. Andersson, M. Bakker, C.M. Plug, M. O'Keeffe, The (twin) composition plane as an extended defect and structure-building entity in crystals, Prog. Solid State Chem. 12 (1979) 273.

[18] A.A. Zhukov, L.E. Shterenberg, V.A. Shalashov, V.K. Thomas, N.A. Berezovskaya, The iron-carbon system. New developments—I. The pseudo-hexagonal iron carbide Fe_7C_3 and the Fe_3C-Fe_7C_3 eutectic, Acta Metall. 21 (1973) 195.

[19] K.H. Jack, Structural transformations in the tempering of high-carbon martensitic steels, J. Iron Steel Inst. 169 (1951) 26–36.

[20] D.H. Jack, Invited review: carbides and nitrides in steel, Sci. Mater. Eng. 11 (1973) 1.

[21] C.M. Fang, M.A. van Huis, H.W. Zandbergen, Structure and stability of Fe_2C phases from density-functional theory calculations, Scr. Mater. 63 (2010) 418.

[22] C.M. Fang, M.A. van Huis, H.W. Zandbergen, Stability and structures of the ε-phases of iron nitrides and iron carbides from first principles, Scr. Mater. 64 (2011) 296.

[23] H. Jang, I.G. Kim, H.K.D.H. Bhadeshia, ε-Carbide in alloy steels: First-principles assessment, Scr. Mater. 63 (2010) 121.

[24] H.I. Faraoun, Y.D. Zhang, C. Esling, H. Aourag, Structural, elastic, and electronic properties of Fe_3C from first principles, J. Appl. Phys. 99 (2006) 093508.

[25] W. Song, J. von Appen, P. Choi, R. Dronskowski, D. Raabe, W. Bleck, Atomic-scale investigation of ε and θ precipitates in bainite in 100Cr6

bearing steel by atom probe tomography and ab initio calculations, Acta Mater. 61 (2013) 7582.

[26] C. Domain, C.S. Becquart, J. Foct, *Ab initio* study of foreign interstitial atom (C, N) interactions with intrinsic point defects in α-Fe, Phys. Rev. B 69 (2004) 144112.

[27] C.M. Fang, M.A. van Huis, H.W. Zandbergen, Structural, electronic, and magnetic properties of iron carbide Fe_7C_3 phases from first-principles theory, Phys. Rev. B 80 (2009) 224108.

[28] W.H. Zhang, W.Q. Lv, Z.P. Shi, S.H. Sun, Z.H. Wang, W.T. Fu, Electronic, magnetic and elastic properties of ε-phases $Fe_3X(X=B, C, N)$ from density-functional theory calculations, J. Mag. Mag. Mater. 324 (2012) 2271.

[29] G. Kresse, J. Hafner, *Ab initio* molecular-dynamics simulation of the liquid-metal–amorphous-semiconductor transition in germanium, J. Phys. Rev. B 49 (1994) 14251.

[30] G. Kresse, J. Furthmüller, Efficient iterative schemes for *ab initio* total-energy calculations using a plane-wave basis set, Phys. Rev. B 54 (1996) 11169.

[31] G. Kresse, J. Furthmüller, Efficiency of ab-initio total energy calculations for metals and semiconductors using a plane-wave basis set, Comput. Mater. Sci. 6 (1996) 15.

[32] P.E. Blöchl, Projector augmented-wave method, Phys. Rev. B 50 (1994) 17953.

[33] G. Kresse, J. Furthmüller, From ultrasoft pseudopotentials to the projector augmented-wave method, Phys. Rev. B 54 (1999) 1758.

[34] J.P. Perdew, K. Burke, M. Ernzerhof, Generalized gradient approximation made simple, Phys. Rev. Lett. 77 (1996) 3865.

[35] C. Amador, W.R. Lambrecht, B. Segall, Application of generalized gradient-corrected density functionals to iron, Phys. Rev. B 46 (1992) 1870.

[36] C.M. Fang, M.A. van Huis, M.H.F. Sluiter, H.W. Zandbergen, Stability, structure and electronic properties of γ-$Fe_{23}C_6$ from first-principles theory, Acta Mater. 58 (2010) 2968.

[37] H.J. Monkhorst, J.D. Pack, Special points for Brillouin-zone integrations, Phys. Rev. B 13 (1976) 5188.

[38] R.E. Cohen, S. Mukherjee, Non-collinear magnetism in iron at high pressures, Phys. Earth Planet. Inter. 143 (2004) 445.

[39] G. Steinle-Neumann, L. Stixrude, R.E. Cohen, Magnetism in dense hexagonal iron, Proc. Natl. Acad. Sci. 101 (2004) 33.

[40] C.M. Fang, M.A. van Huis, J. Jansen, H.W. Zandbergen, Role of carbon and nitrogen in Fe_2C and Fe_2N from first-principles calculations, Phys. Rev. B 84 (2011) 094102.

[41] C.M. Fang, M.A. van Huis, B.J. Thijsse, H.W. Zandbergen, Stability and crystal structures of iron carbides: a comparison between the semi-empirical modified embedded atom method and quantum-mechanical DFT calculations, Phys. Rev. B 85 (2012) 054116.

[42] C.M. Fang, R.A. de Groot, M.M.J. Bischop, H. van Kempen, Oscillatory behavior of the magnetic moments of gold-covered iron surfaces, Phys. Rev. B 58 (1998) 6772.

[43] C. Kittle, Introduction to Solid State Physics, sixth ed., John Wiley and Sons, 2004.

[44] A.W. Hull, A new method of X-ray crystal analysis, Phys. Rev. 10 (1917) 661.